

CAPMix: Robust Time Series Anomaly Detection Based on Abnormal Assumptions with Dual-Space Mixup

Xudong Mou^{1b}, Rui Wang^{1b}, Tiejun Wang^{1b}, Renyu Yang^{1b}, *Member, IEEE*, Shiru Chen^{1b}, Jie Sun^{1b},
Tianyu Wo^{1b}, Xudong Liu^{1b}

Abstract—Time series anomaly detection (TSAD) is a vital yet challenging task, particularly in scenarios where labeled anomalies are scarce and temporal dependencies are complex. Recent anomaly assumption (AA) approaches alleviate the lack of anomalies by injecting synthetic samples and training discriminative models. Despite promising results, these methods often suffer from two fundamental limitations: patchy generation, where scattered anomaly knowledge leads to overly simplistic or incoherent anomaly injection, and Anomaly Shift, where synthetic anomalies either resemble normal data too closely or diverge unrealistically from real anomalies, thereby distorting classification boundaries. In this paper, we propose CAPMix, a controllable anomaly augmentation framework that addresses both issues. First, we design a CutAddPaste mechanism to inject diverse and complex anomalies in a targeted manner, avoiding patchy generation. Second, we introduce a label revision strategy to adaptively refine anomaly labels, reducing the risk of anomaly shift. Finally, we employ dual-space mixup within a temporal convolutional network to enforce smoother and more robust decision boundaries. Extensive experiments on five benchmark datasets, including AIOps, UCR, SWaT, WADI, and ESA, demonstrate that CAPMix achieves significant improvements over state-of-the-art baselines, with enhanced robustness against contaminated training data. The code is available at <https://github.com/alsike22/CAPMix>.

Index Terms—Anomaly detection, anomaly-assumption, anomaly shift, time series, data augmentation

I. INTRODUCTION

Time Series Anomaly Detection (TSAD) aims to identify unusual points or segments that deviate significantly from the normal majority. It plays a crucial role in intelligent applications in various domains. For example, status information is often buried within massive volumes of timestamped data collected from industrial sensors, patient vital signs, network events, and more. Such status information often relates directly

This paper was produced by the IEEE Publication Technology Group. They are in Piscataway, NJ. (Renyu Yang is the corresponding author)

Xudong Mou, Rui Wang, Tiejun Wang, and Xudong Liu are with School of Computer Science and Engineering, Beihang University, Beijing, China. (Email: mxd@buaa.edu.cn, ruiking@buaa.edu.cn, wangtj@buaa.edu.cn, liuxd@buaa.edu.cn)

Renyu Yang and Tianyu Wo are with School of Software, Beihang University, Beijing, China. (Email: renyuyang@buaa.edu.cn, woty@buaa.edu.cn)

Shiru Chen is Shandong Inspur Intelligent Production Technology Co., Ltd, Beijing, 100191, China (Email: chenshiru@inspur.com)

Xudong Liu is also with Zhongguancun Laboratory, Beijing, China.

Manuscript received April 19, 2021; revised August 16, 2021.

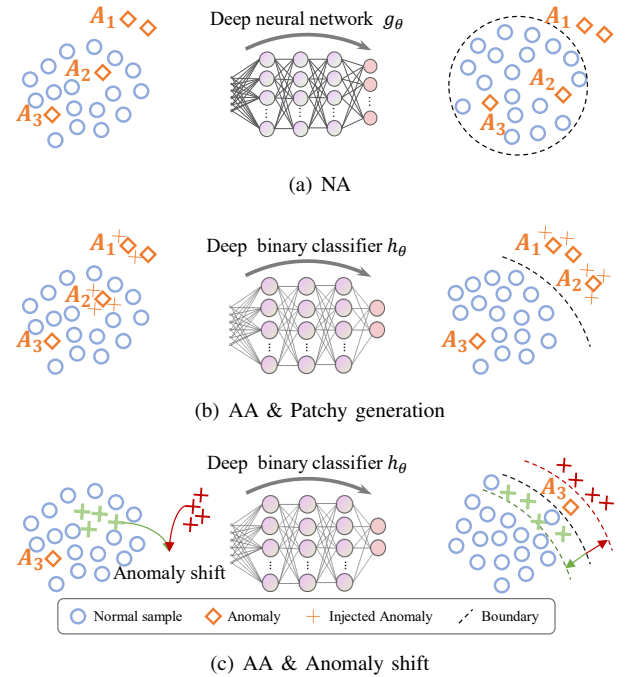


Fig. 1. Schematic of normality and anomaly assumptions used in AD approaches. Anomaly subgroups A_1 , A_2 , and A_3 exist. a) is proficient in identifying anomalies out of distribution, like A_1 . b) could identify anomaly mixed within the normal samples with the aid of augmentations (A_2), but is limited by the scattered augmentation in dealing with A_3 . c) The anomaly shift issue leads to a biased boundary.

to industrial production efficiency, human life and health, or network, and even national security. As anomalies typically constitute only a small fraction of the daily events, manually annotating such rare occurrences in large-scale data is often impractical, if not impossible. Fortunately, the increasing accumulation of large-scale time-series data and advances in deep learning have made unsupervised anomaly detection credible and promising. Notably, the scarcity of labeled anomalies makes TSAD fundamentally different from classification tasks. Moreover, time-series data exhibits unique characteristics such as temporal dependencies, various anomaly types, and complex multivariate relationships, which means that simply adapting mature methods from other domains is often insufficient to tackle TSAD effectively.

Unsupervised approaches dealing with the task of AD

often address the issue of a lack of abnormal samples from two perspectives: normality assumption (NA) and anomaly assumption (AA). As shown in Fig. 1(a), the former assumes normal data should present some characteristics, including single assumptions [1], [2] and fused [3]–[5] ones. The root foundation is the observation that none or only a few anomalous samples are contained in the training set. These methods treat all unlabeled training data as normal and depend on various pretext tasks to learn representations of normal samples, obtaining satisfying results in detecting obvious anomalies, like *A1*. However, inherent semantic information behind some abnormal instances (e.g., a small portion of anomalies annotated by domain experts) within the training set is under-exploited and will lead to inferior detection effectiveness when facing the hidden anomalies or contaminated training data. The other perspective lies in injecting abnormal samples according to the rare knowledge or assumptions of the anomalies to balance the classes of normal and abnormal, then train classifiers as shown in Fig. 1(b) and 1(c). Such studies include Outlier Exposure (OE) [6], CutPaste [7], and Deep SAD [8]. They have achieved promising results in the image domain, but they cannot be directly applied in TSAD.

NCAD [9] and AnomalyBert [10] are among the very few attempts that approach TSAD based on anomaly assumptions. Specifically, NCAD injects random contextual point outliers to simulate anomalies, while AnomalyBert replaces points or distorts subsequences to heuristically cover point- and pattern-wise anomalies [11], although without rigorous justification. As shown in Fig. 1(b), these approaches could separate the hidden *A2* with a coarse using the abnormal knowledge. However, current AA methods often suffer from the distortion challenge, which primarily stems from two issues: patchy generation and *Anomaly Shift*. Patchy generation is rooted in scattered anomaly knowledge, which often leads to weak anomaly injection but ignores complex anomalies like *A3*, reducing detection capacity. For instance, NCAD relies solely on random point anomalies with limited contextual perturbations, overlooking complex pattern-wise anomalies. AnomalyBert conducts random point replacement and subsequent warping without clearly defining the scope of anomalies generated. Meanwhile, the anomaly shift problem occurs when some of the pseudo-anomalies with abnormal labels are either indistinguishable from normal data or deviate unrealistically from real anomalies. This misalignment frequently results in false alarms or missed detections, as shown in Fig. 1(c).

To address these issues, we propose CAPMix, a controllable anomaly augmentation framework for time-series anomaly detection. The key idea is to leverage prior knowledge for anomaly injection, guiding the model to learn stable and smooth classification boundaries. Specifically, we propose CutAddPaste to inject five types of complex anomalies in a targeted manner and apply label revision to better control label assignment. Moreover, by employing a TCN network with dual-space mixup when training on these pseudo-anomalies, the model is encouraged to learn smoother and more robust boundaries, resulting in improved anomaly detection. We conduct extensive experiments on five datasets, including AIOps, UCR, SWaT, WADI, and ESA, and employ Revised Point

Adjusted (RPA) metrics [12] as the performance indicator. Experiment results show that our approach outperforms other baselines in TSAD tasks. In summary, the main contributions of this work are as follows:

- We are the first to incorporate anomaly knowledge into anomaly augmentation methods to guide the complex process of anomaly injection, rather than relying on simple random operations.
- We formally define the problem of *Anomaly Shift*, where some randomly injected anomalies may exhibit low distinctiveness or high deviation, thereby distorting classification boundaries and causing false positives or false negatives.
- We propose a comprehensive framework for time-series anomaly detection, which integrates anomaly injection, label revision, and a dual-space mixing mechanism. This enables controlled complex anomaly injection while mitigating Anomaly Shift, leading to more robust time-series anomaly detection.

This work builds upon CutAddPaste [13], which primarily addressed the challenge of knowledge underutilization, without explicitly tackling anomaly shift. On this basis, we further control the anomaly generation process and refine the classification boundaries when leveraging these anomalies for supervision, thereby achieving improved anomaly detection performance, with an improvement of approximately 25% on multivariate time-series datasets.

The remainder of this paper is organized as follows. First, we summarize the related work on time series anomaly detection based on deep learning. Then we illustrate the methodology in detail, including the overall framework and each component. Next, we design several experiments to study the effect of the whole approach and its components, report, visualize, and analyze the experimental results. Finally, we conclude this paper and discuss future work.

II. RELATED WORK

Research on time series anomaly detection has evolved along multiple directions. In this section, we briefly review three lines of work that are most relevant to our approach: methods based on the normality assumption [14], methods leveraging anomaly injection or anomaly assumptions, and strategies involving sample mixing to enhance distribution alignment and model robustness. Table I details the comparison between our method and other related work from different perspectives.

Normality assumption based methods. Normality assumption based approaches assume that the majority of the training data is normal. They build representations of so-called *normality*, i.e., using GANs [15], [16], autoencoder [1], one-class [2], and clustering [17] methods. Data that does not obey these representations is considered abnormal. While they provide diverse insights into normality (such as can be better reconstructed), they may entail certain limitations and biases in capturing their entirety. Some researchers integrate assumptions for better-encompassing normal features. For example, [18] extracts a representation of the entire dataset

TABLE I
COMPARISON OF RELATED WORK.

Method	Domain	N	A ¹	Anomaly Shift ²		TS Anomaly Type				
				Close	Far	Global	Contextual	Shapelet	Seasonal	Trend
Deep SVDD [2]	Image	✓	×	-	-	×	×	×	×	×
RoCA [5]	TS	✓	×	-	-	×	×	×	×	×
OE [6]	Image	✓	✓	×	×	×	×	×	×	×
CutPaste [7]	Image	✓	✓	×	×	×	×	×	×	×
DeepSAD [8]	Image	✓	✓	×	×	×	×	×	×	×
NCAD [9]	TS	✓	✓	×	×	✓	✓	×	×	×
AnomalyBert [10]	TS	✓	✓	×	×	✓	✓	×	×	×
GenIAS [19]	TS	✓	✓	✓	×	✓	✓	✓	✓	✓
RedLamp [20]	TS	✓	✓	✓	×	✓	✓	✓	✓	✓
CAPMix	TS	✓	✓	✓	✓	✓	✓	✓	✓	✓

¹ N and A represent whether the method uses normal and abnormal samples.

² “Close” means addressing the normal-like synthetic anomalies, and “Far” means avoiding generating excessive outliers.

and leverages the intrinsic normality to identify anomalies in two separate stages. COCA [3] and RoCA [5] combine some preceding assumptions into an all-encompassing one to eliminate the potential negative impact of features extraneous to AD. However, it remains unclear whether such integration truly captures the full extent of normality, and excessive fusion may even hinder model convergence. Moreover, underutilizing prior anomaly knowledge leaves the model to learn from scratch, limiting its effectiveness.

Anomaly assumption based methods. While normality might prove elusive, researchers possess some insight into abnormal states. They harness random pseudo-anomalies to train classifiers. Outlier Exposure (OE) [6] integrates data from external datasets during training, exposing the model to out-of-distribution instances to learn a more conservative concept of normal samples, and thus can boost the detection of uncharted anomaly patterns. Deep Semi-supervised Anomaly Detection (Deep SAD) [8], an extension of Deep SVDD [2], incorporates known anomalies in the model and can exhibit a higher cross-entropy within the latent distribution than normal samples. In the Computer Vision (CV) context, CutPaste [7] employs data augmentation techniques – e.g., involving the excision of an image patch and placement in a random location of a larger image and producing spatial irregularities – to offer a rudimentary simulation of image defects. [21] demonstrates that relatively few random OE samples are necessary to yield state-of-the-art detection performance.

NCAD [9] adapts the OE approach to time series scenarios by infusing mixed contextual and random point anomalies into the time series data, for establishing a discerning boundary between normal and anomalous classes. However, it fails in providing pattern-wise anomalies, which is a large category of time series anomalies, underscoring the importance of domain knowledge. AnomalyBert [10] roughly attempts to replace points or distort subsequences to cover point heuristically, and pattern-wise anomalies. GenIAS [19] generates abnormal patches with VAE while trying to avoid generating normal samples. RedLamp [20] uses twelve augmentations to generate anomalies and perform a task of multi-classification. It additionally uses label refurbishment to enhance its robustness against false anomalies and anomaly contamination. However, they mainly target the risk of misclassifying normal samples as anomalies, focusing on correcting labels for potentially

normal-like instances. In contrast, our CAPMix not only revises labels using a distance-based criterion but also constrains the risk of generating unrealistically abnormal samples through a configurable dual-space Mixup. This ensures better alignment with the true anomaly distribution and mitigates the issue of anomaly shift.

Mixup. Mixup-based data augmentation has proven to be powerful in computer vision, with a series of extensions refining the mixing mechanism to generate more meaningful and label-faithful samples. [22] first proposed MixUp, which linearly interpolates two images and their labels in a convex combination, regularizing neural networks by encouraging smoother decision boundaries. Building on the original MixUp, subsequent variants such as CutMix [23], SnapMix [24], and SmoothMix [25] have progressively refined the mixing mechanism to generate more realistic, semantically consistent, and diverse samples. These strategies mainly aim to address issues like unnatural boundaries, inaccurate label assignment, and limited representativeness, thereby enhancing the robustness and generalization ability of image recognition models. On the other hand, manifold mixup [26] introduces novel concepts for mixing within the representational space and also inspires our dual-space mixing methodology. In the time series domain, [27] learns better time-series representations for classification tasks by mixing both phase and amplitude components, while TimeMixer++ [28] implements mixing across multiple scales. However, these methods only perform mixing in the sample space and often serve to improve the robustness of classification tasks, rather than anomaly detection based on anomaly assumptions.

III. METHODOLOGY

This section details the proposed CAPMix framework. We first formulate the problem and highlight the *Anomaly Shift* issue. Then, we describe the pipeline consisting of anomaly injection, label revision, and dual-space mixup, followed by the optimization objectives.

A. Problem Definition

Given an ordered time series $\mathcal{S} = \{x_1, x_2, \dots, x_l\}$ collected during an l -length time period. $x_i \in \mathbb{R}^d$ is a d -dimensional vector collected at timestamp i . The time series will be

denoted as univariate if $d = 1$, and as multivariate if $d > 1$. Conventional approaches typically split the long time series \mathcal{S} into a set of time subsequences, i.e., $\mathcal{D} = \{\mathbf{X}_1, \mathbf{X}_2, \dots, \mathbf{X}_N\}$ by sliding windows whose length is set to be t . A sample $\mathbf{X}_i = \{x_1, x_2, \dots, x_t\}$ is the collection of points within a time subsequence, and N is the number of samples. Time step $\delta \leq t$ is the stride of sliding, where the samples are overlapping if $\delta < t$. To better describe the characteristics of pattern-wise anomalies, we adopt structural modeling [11] to represent a time-series sample as $X = \Gamma(2\pi\omega T) + \Theta(T)$, where $T = \{1, 2, \dots, t\}$. Γ defines the basic shapelet function, which not only describes the shape of the time series but also includes relationships between various dimensions. These relationships can be depicted by a covariance matrix $cov(X, X)$. ω is the seasonality and Θ is the trend function describing the direction of X_i . Correspondingly, \mathcal{D} has a set of labels $\mathcal{Y} = \{y_1, y_2, \dots, y_N\}$ with $y_i \in \{0, 1\}$ indicating that the sample \mathbf{X}_i is normal (0) or anomalous (1). The goal is to predict a label $\hat{y}_i \in \{0, 1\}$ given a time series \mathbf{X}_i . We calculate an anomaly score S_i instead of giving the binary labels directly, and a predicted label can be obtained by comparing S_i to a predefined threshold τ .

B. Anomaly Shift Problem

In the context of time series anomaly detection, methods based on anomaly assumptions generate synthetic anomalies to augment training data and improve the robustness of the model. Although this approach has shown promise, we identify a critical issue that hinders its effectiveness: the anomaly shift problem. This issue occurs when generated anomalies deviate significantly from the actual distribution of abnormal patterns, leading to several complications:

- Low distinctiveness: generated anomalies are too close to the normal data, making them indistinguishable from genuine normal samples. This ambiguity weakens the anomaly-normal separation, reducing detection reliability.
- High deviation: generated anomalies deviate excessively from the true data manifold. While seemingly “different,” such unrealistic anomalies fail to provide meaningful supervision and may even enlarge the decision boundary unnecessarily, leading to false alarms on normal samples. These anomalies essentially become outliers in the feature space, far from both normal and abnormal data distributions.

To highlight this problem, we illustrate the anomaly shift in Fig. 2. In (a), anomalies are overly similar to the normal data, leading to misclassification as normal. In (b), anomalies are injected too far from the real data distribution, resulting in poor boundary generalization. However, it is often not so easy to evaluate the rationality of anomaly injection.

To formalize this problem, let $\mathcal{X}_{norm} \sim \mathcal{D}_{norm}$ and $\mathcal{X}_{real}^a \sim \mathcal{D}_{real}$ denote the normal and real anomalous samples, respectively. Synthetic anomalies $\mathcal{X}^a \in \mathcal{D}_{syn}$ are introduced to balance the classifier. Anomaly shift arises when $\mathcal{D}_{real} \neq \mathcal{D}_{syn}$, resulting in the distributional gap:

$$\mathcal{D}_{shift} := Dist(\mathcal{D}_{real}, \mathcal{D}_{syn}) > \epsilon, \quad (1)$$

where $Dist$ is a divergence measure, and $\epsilon > 0$ denotes a tolerable threshold. This distributional discrepancy causes a mismatch between training and testing objectives. Specifically, the model minimizes the empirical loss:

$$\mathcal{L}_{train} = \mathbb{E}_{X \sim \mathcal{D}_{norm}} [\ell(f_\theta(X), 0)] + \mathbb{E}_{\hat{X} \sim \mathcal{D}_{syn}} [\ell(f_\theta(\hat{X}), 1)], \quad (2)$$

while the test-time performance depends on:

$$\mathcal{L}_{train} = \mathbb{E}_{X \sim \mathcal{D}_{norm}} [\ell(f_\theta(X), 0)] + \mathbb{E}_{X \sim \mathcal{D}_{f \setminus \setminus}} [\ell(f_\theta(X), 1)]. \quad (3)$$

Therefore, a key challenge is to bridge the anomaly shift by generating more realistic anomalies or designing learning mechanisms that are resilient to such shifts, which we address in the next part.

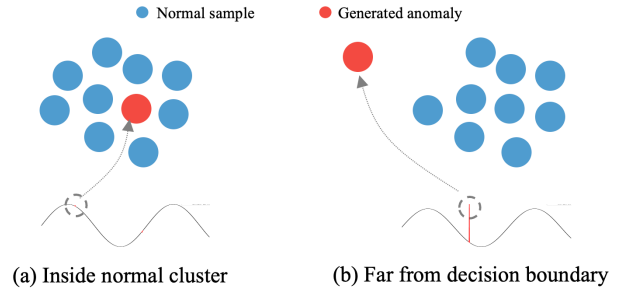


Fig. 2. Schematic diagram of Anomaly Shift.

C. CAPMix Overview

To tackle the issues of patchy generation and anomaly shift, we propose CAPMix. The intuitive insight is to deliberately disrupt temporal dependencies within sequences and correlations across dimensions, thereby injecting structured anomalies into the data. In addition, CAPMix incorporates label revision to prevent near-normal augmented samples from being incorrectly assigned hard anomaly labels, while dual-space mixup avoids generating overly unrealistic anomalies. Together, these two mechanisms effectively mitigate the anomaly shift problem, enabling the classifier to learn smoother and more reliable decision boundaries. As Fig. 3 shows, the proposed CAPMix is a structured anomaly detection framework that progressively transforms input time series into meaningful anomaly scores via multi-level operations. The process is organized as a left-right flow, including anomaly injection, label revision, classification, and loss-based optimization.

Starting from raw time-series input, our model injects sparse but informative synthetic anomalies using the controlled base method. These enriched sequences are then processed to revise the labels according to dynamic time warping (DTW) distance and exclude the effect of anomaly shift. Then, the revised samples are fed into the CAPMix model to pass through a series of dual-space mixup and Temporal Convolutional Network (TCN) blocks, which collaboratively learn robust temporal representations by interpolating and transforming features across both input and latent spaces. Finally, the classifier projection predicts anomaly probabilities used to compute the binary cross-entropy (BCE) loss, guiding the model optimization.

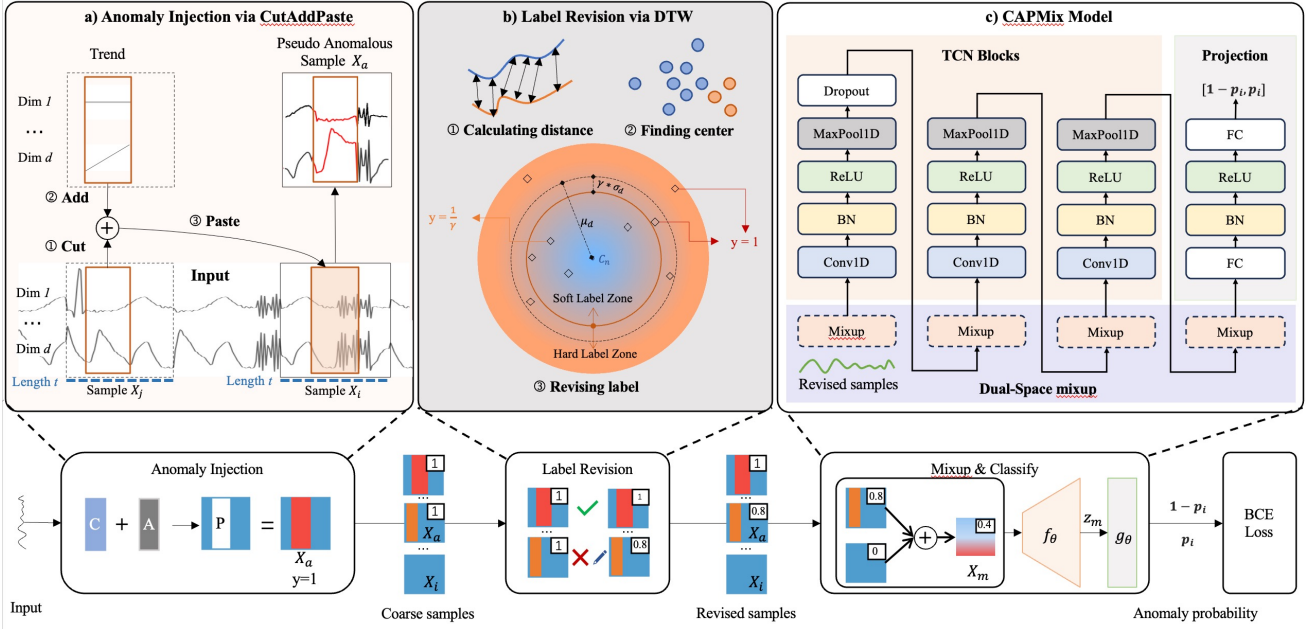


Fig. 3. The overview of CAPMix, composed of three main components: a) Generation with CutAddPaste, which produces diverse synthetic anomalies by injecting patches into normal sequences. b) Label Revision, which recalibrates the labels of generated anomalies based on their distances to the normal center, reducing mislabeling caused by overly normal-like samples. c) Dual-Space Mixup, which applies Mixup operations in both the input and latent feature spaces to encourage robust and consistent decision boundaries.

D. CAPMix Pipeline

Anomaly Injection via CutAddPaste. We propose the CutAddPaste approach to generate abnormal samples encompassing both point-wise and pattern-wise anomalies. This method extends CutPaste [7] from the image domain to time series by adopting a window-based mechanism for greater efficiency. Beyond shape- and season-related anomalies, it introduces a crucial trend component to additionally model trend, correlation, and point-wise anomalies. Specifically, after partitioning the original series \mathcal{S} into equal-length segments via sliding windows, CutAddPaste synthesizes anomalous patches and substitutes them into random positions of a given sample X_i , effectively replacing its original values. As illustrated in Fig. 4, the process involves the following three steps to generate samples covering all five types of anomalies.

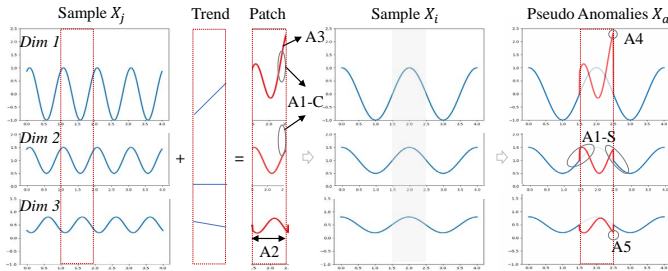


Fig. 4. Example of generating an anomalous sample over sine waves. The original $\text{Dim}2 = 0.5 \cdot \text{Dim}1 + 1$. There are pattern-wise anomalies in terms of shapelet (A1-S: shape, A1-C: correlation), seasonality (A2), and trend (A3). Point-wise anomalies include global (A4) and contextual (A5) ones.

- **Cut:** It cuts a patch of randomly sized $r \geq \zeta$ subsequence from another arbitrarily chosen sample X_j , where the

hyperparameter $\zeta \in (0, t)$ controls the minimum length of the patch, as the length has to be long enough to generate an anomaly.

- **Add:** It adds a series of incremental or decremental values V_{trend} deriving from a linear function with a random slope to the patch. For multivariate time series, it selectively chooses and aggregates some of these dimensions to form random trends and adds them to the cut patch.
- **Paste:** It embeds the patch into a random position of sample X_i . The value from the patch replaces the pre-existing value within this location.

Formally, given the paste (destination) sample $\mathbf{X}_i = \Gamma_i(2\pi\omega_i T) + \Theta_i(T)$ and the cut (source) sample $\mathbf{X}_j = \Gamma_j(2\pi\omega_j T) + \Theta_j(T)$, where $T = \{1, 2, \dots, t\}$. \mathbf{X}_i and \mathbf{X}_j come from \mathcal{S} , which has been standardized. The trend item $V_{trend} = \rho \cdot m \cdot R$, where $R = \{1, 2, \dots, r\}$. $m = (m_1, m_2, \dots, m_d)$ is a d -dimensional random slope vector, where $-1 < m_i < 1$. Hyperparameter $\rho > 0$ controls the degree of the trend term. After the above augmentation, the pseudo-abnormal sample \mathbf{X}_a is defined as: $\{x_b | b \in T\}$, and the formulation of X_a involving X_i , X_j , and \mathbf{V}_{trend} is depicted as follows:

$$x_b = \begin{cases} \Gamma_i(2\pi\omega_i b) + \Theta_i(b), & b \in \{1, \dots, k_i - 1\} \\ \Gamma_j(2\pi\omega_j(b+k)) + \Theta_j(b+k) + \rho m(b-k'), & b \in \{k_i, \dots, k' + r\} \\ \Gamma_i(2\pi\omega_i b) + \Theta_i(b), & b \in \{k_i + r, \dots, t\}, \end{cases} \quad (4)$$

where $k = k_j - k_i$, $k' = k_i - 1$. $k_i < t - r$ and $k_j < t - r$ are the random pasting position and cutting position, respectively. As illustrated in Fig. 4, considering the subsequence $X[t_1 : t_2]$,

i.e., $\{x_{t_1}, x_{t_1+1}, \dots, x_{t_2}\}$, we formulate the following relevant five types of anomalies onto X_a :

- **A1-S: Shape.** Generally, Γ_i is different from Γ_j because X_j is chosen randomly. Therefore, an arbitrary sub-sequence $X_a[t_1 : t_2]$ from $t_1 \in [1 : k_i]$ to $t_2 \in [k_i + 1, T]$ contains at least one hop transition of the shape function Γ , forming the shape anomalies.
- **A1-C: Correlation.** For X_i , the original relationships among the multiple variables are defined as $cov(X_i, X_i) = E[(X_i - E[X_i])(X_i - E[X_i])^T]$. Because the i -th slope m_i is an independently generated random number, $E[X_a]$ will deviate from $E[X_i]$, further causing $cov(X_a, X_a) \neq cov(X_i, X_i)$, i.e., correlation anomalies.
- **A2: Seasonality.** The seasonality parameter of the patch $X_a[k_i : k_i + r - 1]$ is ω_j rather than the expected ω_i .
- **A3: Trend.** After the augmentation, the trend function of the patch $\Theta_a = \Theta_j + V_{trend}$, which is different from the expected Θ_i .
- **A4 & A5: Point-wise.** When $b = k' + r$, $x_b = X_j[k_j + r - 1] + pmr$. If $m_i \neq 0$, such as *Dim1* and *Dim3* in Fig. 4, x_b is proportional to r . Therefore, when r is large enough, $|x_b - \mu|$ will exceed the 3σ to create a global (A4) or contextual (A5) anomaly, where μ and σ are the mean and standard deviation of the whole time series S or the neighborhood points.

Label Revision via DTW. As discussed, the anomaly shift issue introduces the risk of label misalignment: injected samples may not fully exhibit clear abnormal features, yet are assigned one-hot labels. The one-hot labels can be too coarse to guide the model in learning a meaningful decision boundary. We propose a label-revision mechanism that leverages the DTW distance to mitigate label uncertainty. Specifically, we compute each generated sample's DTW distance to the normality center. The soft labels between 0 and 1 are selected accordingly, indicating the likelihood of the anomaly based on similarity.

We first estimate the normality center C_n of the training data, assuming that the majority of the training set is normal. Given a collection of normal sequences $\mathcal{D} = \{X_1, X_2, \dots, X_N\}$, the center is computed as the mean sequence over all time steps:

$$C_n = \frac{1}{N} \sum_{i=1}^N X_i. \quad (5)$$

For each generated sample X_a , we compute its DTW distance $d(X_a, C_n)$ to C_n . Denote the mean and standard deviation of distances from the original training samples to C_n as μ_d and σ_d . Then we define a soft label zone bounded by:

$$[0, \mu_d - \gamma \cdot \sigma_d], \quad (6)$$

where $\gamma \geq 0$ is a tunable hyperparameter controlling the soft region's width. Samples falling within this zone are likely to resemble normal patterns and are therefore assigned a soft anomaly label y_r of $1/\gamma$. In contrast, samples falling outside this boundary are considered confidently abnormal and

assigned a hard label y_r of 1. Then the original label set is refined as \mathcal{Y}_r . Formally, each label y_r in \mathcal{Y}_r is:

$$y_r = \begin{cases} 1, & \text{if } d(X_{\text{syn}, C_n}) > \mu_d + \gamma \sigma_d \\ \frac{1}{\gamma}, & \text{otherwise.} \end{cases} \quad (7)$$

Although defining different soft labels based on the distance ratio $d/(\mu_d - \gamma \cdot \sigma_d)$ might seem more intuitive, the high computational cost associated with this approach leads us to opt for the controlled label $1/\gamma$. This assignment scheme avoids the instability of assigning continuous labels solely based on raw distance values.

DualSpace Mixup Integrated TCN. In addition to the label revision mechanism that mitigates the risk of assigning overly confident labels to normal-like synthetic samples, another fundamental concern arises: the possibility that generated anomalies become unrealistically abnormal, deviating from plausible anomaly distributions. To tackle this issue, we introduce a Dual-Space Mixup strategy, integrated within a TCN framework, which regularizes the model across both the input space and latent space.

The proposed CAPMix model employs a three-block TCN to convert t -sized X_i into a fixed-size vector representation z_i . It is achieved by three temporal convolutional blocks $f^{(l)}(\cdot)$, where $l \in [1, 2, 3]$. Each block comprises a Conv1D layer, a Batch Normalization (BN) layer, a ReLU activation function, and a MaxPool1D layer. The first block contains an additional Dropout layer. We apply mixup operations between the layers:

$$\begin{aligned} X_{Mix}^{(l)} &= \lambda \cdot f^{(l)}(X_i) + (1 - \lambda) \cdot f^{(l)}(X_j), \\ y_{Mix}^{(l)} &= \lambda \cdot y_i^{(l)} + (1 - \lambda) \cdot y_j^{(l)}, \end{aligned} \quad (8)$$

where $y^{(l)}$ is the label given by the l -th layer mixup block. In particular, the first mixup layer is in the input space, where $l = 0$.

$$\begin{aligned} X_{Mix}^{(0)} &= \lambda \cdot X_i + (1 - \lambda) \cdot X_j, \\ y_{Mix}^{(0)} &= \lambda \cdot y_i + (1 - \lambda) \cdot y_j. \end{aligned} \quad (9)$$

The model thus supports a layer-wise configurable integration of Mixup, controlled by a flexible setting to switch on/off Mixup at each level, making the design extensible and adaptable.

The representation z_i is fed into a learnable nonlinear projector $g_\theta : \mathcal{C} \mapsto \mathcal{Q}$ to output the projection q_i . The projector applies an MLP with one hidden layer that uses BN and ReLU activation functions. It maps representations obtained from the feature encoder into a 2-dimensional projection space. This mapping is guided by calculating the binary cross-entropy loss, which will be detailed in Section III-E

Denoting the revised synthetic anomaly distribution as $\hat{\mathcal{D}}_{\text{syn}}$ after applying DTW-based soft labeling and dual-space Mixup, we claim that

$$\text{Dist}(\mathcal{D}_{\text{real}}, \hat{\mathcal{D}}_{\text{syn}}) < \text{Dist}(\mathcal{D}_{\text{real}}, \mathcal{D}_{\text{syn}}), \quad (10)$$

which will be proved in the visualization part of our experiments.

E. Model Training Objective

Finally, the loss is obtained by calculating the projection q_i and the label y_i . Inspired by hypersphere classification (HSC) [6], [21], we use the binary cross-entropy loss as the training objective.

Algorithm 1 CAPMix pipeline.

Input: a set of subsequence samples $\{\mathbf{X}_i\}_{i=1}^B$, labels $\{y_i\}_{i=1}^B$

Parameter: batch size B , window size t , structure of f, g , constant $\rho, \zeta, v, e, \gamma$

Output: network f, g

```

1:  $\mathbf{X}' = \mathbf{X}.\text{copy}()$ 
2: for all  $i \in \{1, \dots, B\}$  do
3:    $r = \max(\text{int}(\zeta), \text{int}(\text{random.random()} \times t))$ 
4:    $\text{cut\_position} = \text{int}(\text{random.uniform}(0, t - r))$ 
5:    $\text{paste\_position} = \text{int}(\text{random.uniform}(0, t - r))$ 
6:    $j = \text{int}(\text{random.uniform}(0, B))$ 
7:    $\text{cut\_data} = X_j[\text{cut\_position}, \text{cut\_position}+r]$ 
8:    $\text{trend} = \{1, 2, \dots, r\}$ 
9:   if  $\text{cut\_data.shape}[1] \geq 1$  then
10:     $\text{dim\_all} = \{0, \dots, \text{cut\_data.shape}[1] - 1\}$ 
11:     $\text{dim} = \text{random.choice}(\text{dim\_all}, \text{size}=e)$ 
12:   else
13:     $\text{dim} = \{0\}$ 
14:   for all  $\text{item} \in \text{dim}$  do
15:     $\text{factor} = \text{random.random()} \times \rho$ 
16:     $\text{add} = \text{random.choices}([-1, 1]) \times \text{factor} \times \text{trend}$ 
17:     $\text{cut\_data}[:, \text{item}] += \text{add}$ 
18:    $\mathbf{X}'_i[\text{paste\_position}, \text{paste\_position}+r] = \text{cut\_data}$ 
19:  $\text{anomaly\_num} = \text{int}(v \times B)$ 
20:  $\mathbf{X}' = \text{random.sample}(\mathbf{X}', \text{anomaly\_num})$ 
21:  $y' = \text{torch.ones}(\text{anomaly\_num})$ 
22:  $C_n = \frac{1}{N} \sum_{i=1}^N X_i$ 
23: for all  $\mathbf{X}'_i \in \mathbf{X}'$  do
24:    $d(\mathbf{X}'_i) = d(\mathbf{X}'_i, C_n)$ 
25:   if  $d(\mathbf{X}'_i) > \mu_d + \gamma \cdot \sigma_d$  then
26:      $y'_i = 1/\gamma$ 
27:  $\mathbf{X} = \text{cat}((\mathbf{X}, \mathbf{X}'), \text{axis}=0)$ 
28:  $y = \text{cat}((y, y'))$ 
29: for sampled batch  $\{\mathbf{X}_i\}_{i=1}^N$  do
30:   for all  $i \in \{1, \dots, N\}$  do
31:      $q_i = g(f(\mathbf{X}_i))$ 
32:      $p_i = q_i[1]$ 
33:    $\mathcal{L} = -\frac{1}{N} \sum_{i=1}^N [y_i \cdot \log(p_i) + (1 - y_i) \cdot \log(1 - p_i)]$ 
34:   update networks  $f, g$  to minimize  $\mathcal{L}$ 
35: return network  $f, g$ 

```

The projector g_θ outputs the 2-dimensional projections $\mathcal{Q} = \{q_1, \dots, q_i, \dots, q_N\}$, and *softmax* maps q_i to a pair of probabilities $[1 - p_i, p_i]$, where p_i and $1 - p_i$ represent the probability of being anomalous and being normal, respectively. We use *softmax* instead of *sigmoid* to obtain the two probabilities, separately. The binary cross-entropy loss is defined

as:

$$\mathcal{L} = -\frac{1}{N} \sum_{i=1}^N [y_i \cdot \log(p_i) + (1 - y_i) \cdot \log(1 - p_i)], \quad (11)$$

where y_i is the label in \mathcal{Y}_r . For the training set with labels, \mathcal{Y}_r contains the original labels annotated by domain experts and our labels corresponding to the pseudo-anomalous samples. It is worth mentioning that our method does not require the training set to contain anomalies. As shown in Table III, CAPMix performs well on UCR, SWaT, and WADI, all of which are generic training sets without anomalies. The pseudo-code of CAPMix in Pytorch style is provided in Algorithm 1.

In the test phase, we consider the probability p_i of the subsequence sample \mathbf{X}_i as the anomaly score $S_i \in [0, 1]$. Then, we use the following standard to determine whether \mathbf{X}_i can be classified as anomalous:

$$x_i = \begin{cases} \text{anomaly}, & S_i > \tau \\ \text{normal}, & S_i \leq \tau \end{cases}, \quad (12)$$

where τ is a predefined threshold.

IV. EXPERIMENTS

In this section, we outline the experiment setup, implementation specifics, primary outcomes, ablation research, visualization, and hyperparameter analysis. The code is available at <https://github.com/alsike22/CAPMix>.

A. Experiment Setup

This part introduces the experimental setup, including the datasets, evaluation metrics, and baselines.

Datasets. In light of [29], the evaluation is conducted on AIOps, UCR, SWaT, WADI, and ESA datasets, eschewing flawed time-series AD datasets like Numenta [30], Yahoo [31], NASA (SMAP and MSL) [12], and SMD [32]. Dataset details are as follows.

- **AIOps** [33], which is also called the “KPI” dataset, is comprised of 29 univariate time-series sub-datasets. It includes well-maintained business cloud key performance indicators from several prominent Internet companies. Most of the anomalies are point-wise, which can be observed in Fig. 6(a).
- **UCR** [29] is also a univariate dataset, containing 250 sub-datasets involving multiple domains, such as human health and sensors. On each sub-dataset, UCR contains only 1 anomaly segment, which means it could not provide anomalous samples in the training set. Most of the anomaly segments are pattern-wise anomalies.
- **SWaT** [34] is a multivariate dataset from the Secure Water Treatment (SWaT) testbed under normal and attacked behavioral modes. It contains only one subset that encompasses signals from 51 sensors. The anomalies turn out to be long-term and pattern-wise.
- **WADI** [35] is a high-dimensional extension of SWaT on the testbed, consisting of signals from 123 sensors and actuators. The pattern-wise anomalies are shorter than those on SWaT.

TABLE II
SUMMARY OF TSAD DATASETS. TRA-ANO IS THE PROPORTION OF
ANOMALIES IN THE TRAINING SET.

	AIOps	UCR	SWaT	WADI	ESA
Subsets	29	250	1	1	1
Variables	1	1	51	127	6
Domain	Cloud KPIs	Various	Waterworks	Waterworks	Satellite
Length	32	64	32	32	256
Time step	32	16	16	16	256
Training	93864	330583	29699	49034	12273601
Validation	18251	175564	5624	2160	2454720
Testing	91201	877355	28118	10799	9818879
Anomalies	3.59%	0.53%	5.96%	1.06%	0.75%
Tra-Ano	3.86%	0%	0%	0%	0.6%

- **ESA** [36] is a large multivariate dataset from the European Space Agency that contains annotated real-life telemetry from three different missions. It avoids the dataset issues proposed in [29]. Due to the large amount of data, this article utilizes Mission 1 of the dataset and employs a minimum of six dimensions, as recommended by the dataset. Rare events are regarded as anomalies.

As demonstrated in Table II, each time series (subset) is segmented into length- t sequences using a sliding window with a time-step δ . In addition, the table presents the sequence count in the training, validation, and testing sets and the proportion of anomalous samples in the whole dataset and training set. The AIOps dataset includes a higher proportion (Tra-Ano) of anomalies in the training set, implying that the training data is contaminated, as the CAPMix approach operates in an unsupervised manner.

Metrics. Evaluation metrics of time series anomaly detection have been blurring for a long time. On the one hand, the intuitive metric of Point-Wise (PW) is underestimating the model's ability to detect anomalous segments, since most detection results could not be well aligned with the ground truth anomaly segments. It could be fair while evaluating the methods on point anomalies. On the other hand, metrics favor anomalous segments tend to overestimate the model's capabilities. For instance, the popular Point Adjusted (PA) [37] considers that if even a single point is detected as anomalous, the entire segment is predicted correctly.

By summarizing previous work [3]–[5], [12], [38], [39], this paper employs the Revised Point-Adjusted (RPA) metric [12] for the sake of fairness. In addition, for the datasets consisting of multiple subsets (AIOps and UCR), the reported results are computed on the entire dataset, which is a weighted average of the RPA F1-score for each sub-dataset:

$$F1_{\text{entire}} = \sum_{i=1}^M \frac{e_i}{E} F1_i, \quad (13)$$

where M is the number of sub-datasets, E is the total count of anomalies (including points and segments) of the entire dataset, and e_i is the number of anomalies of the i -th sub-dataset.

Baselines. The proposed CAPMix is compared against several traditional, normality assumptions-based, and anomaly assumptions-based AD methods that are listed below.

Traditional AD Baselines. Five commonly used traditional AD methods are adopted: One-Class SVM (OC-SVM) [40],

Isolation Forest (IF) [41], Robust Random Cut Forest (RRCF) [42], Spectral Residual (SR) [43], and DAMP [44]. For the large ESA-TAD dataset, the simple baselines are revised to handle large windows. Inspired by [38], we design a simple baseline: the Randomized Anomaly Score (RAS), which takes a random decimal value in the range of 0 to 1 as the anomaly score.

Normality Assumptions-based AD Baselines. Then, six single and three multiple deep normality assumptions-based AD methods are compared: LSTM Encoder-decoder (LSTM-ED) [1], Deep one-class (Deep SVDD) [2], Anomaly Transformer [46], MixMamba [47], MTSCAD [48], and SensitiveHUE (SensHUE) [49] are based on single assumptions involving reconstruction, one-class classification, and prediction. RoCA [3], AOC [4], and TCC [18], [45] are based on multiple assumptions.

Anomaly Assumptions-based AD Baselines. Finally, three anomaly assumptions-based method is set: NCAD [9], AnomalyBert [10], and CutAddPaste [13]. NCAD offers supervised and unsupervised settings for the AIOps dataset, but the former yields better AD performance and serves as the baseline for this paper. AnomalyBert and CutAddPaste inject abnormal patches into the original samples with different approaches. Among them, Deep SVDD was originally designed for AD in images but provides significant underlying concepts. Therefore, previous work [3], [4], [9] adopted Conv1D as its autoencoder part to migrate it to the time series domain.

Regarding TCC based on [18], we conduct representation learning during the pre-training phase using TS-TCC [45] and anomaly detection during fine-tuning with the principles of Deep SVDD.

B. Implementation Details

The 1D-CNN of the TCN encoder has a dropout rate of 0.45. We adopt a learning rate from $1e-4$ to $5e-4$, weight decay of $5e-4$, $\beta_1 = 0.9$, and $\beta_2 = 0.99$ in an Adam optimizer. Since each time series in UCR has only one anomaly segment, we choose the sample with the largest anomaly score as the location of the anomaly. In addition, we perform the early stopping strategy on UCR, as the time series from different domains vary in epochs to convergence. For the other datasets, the obtained raw anomaly scores are converted into Z-scores, and we search for the optimal anomaly threshold $\tau \in [-3, 3]$ according to the 3σ -rule. For robust results, each approach is executed 10 times with different random seeds, and we calculate the mean and standard deviation of the metrics. The models are implemented using PyTorch 1.7 and Merlion 1.1.1 [50], and trained on an NVIDIA Tesla V100 GPU.

C. Main Results

We report the AD performance of the baselines and our method in Table III.

TSAD performance. From the perspective of the datasets in Table III, there are the following three key observations. Firstly, there is significant variation in the AD performance of methods like OC-SVM, AAS, and COCA across the AIOps

TABLE III
MAIN RESULTS¹.

Method \ Dataset	Univariate Datasets			Multivariate Datasets			
	AIOps	UCR	Average	SWaT	WADI	ESA	Average
OC-SVM [40]	7.02	16.42	11.72	0.02	0.03	29.79	9.95
IF [41]	3.86±0.07	4.51±0.44	4.19±0.26	12.79±1.94	0.87±0.16	8.61±0.39	7.42±0.83
RRCF [42]	2.89±0.06	5.91±0.67	4.40±0.37	0.99±0.05	0.95±0.09	6.43±1.72	2.79±0.62
SR ² [43]	8.52	22.00	15.26	-	-	-	-
DAMP [44]	2.72	39.03	22.10	0.70	0.18	9.09	3.32
RAS [38]	5.46±0.83	20.88±3.06	13.17±1.95	10.30±2.00	9.77±3.55	1.60 ± 0.58	7.22±3.07
LSTM-ED [1]	14.05±0.52	24.64±1.11	19.35±0.82	5.48±0.04	3.86±0.52	<u>54.80±2.92</u>	21.38±1.53
Deep SVDD [2]	25.53±7.38	48.34±2.74	36.94±5.06	8.88±6.97	6.14±2.09	5.16±1.83	6.73±3.63
AOC [4]	41.40±3.28	20.99±0.78	31.39±2.04	27.59±0.02	0.36±0.01	22.38±1.41	16.78±0.48
TCC [18], [45]	3.03±0.66	2.53±0.75	2.78±0.71	2.06±0.66	5.02±3.79	0.45±0.32	2.51±1.59
AnoTrans [46]	0.38±0.13	6.01±1.26	3.20±0.70	32.91±1.19	1.68±0.02	5.54±0.65	13.38±0.62
MixMamba [47]	16.72±0.12	12.88±0.56	15.14±0.68	2.39±0.07	4.66±0.39	0.30±0.03	2.45±0.16
MTSCAD [48]	57.24±1.20	10.04±0.97	33.64±1.09	19.70±0.43	4.30±3.44	0.55±0.72	8.20±1.51
RoCA [5]	50.14±5.08	55.64±2.59	52.18±2.59	21.05±5.11	14.45±6.93	31.41±22.64	22.30±11.56
NCAD [9]	41.06±3.32	22.24±2.99	31.65±3.16	7.54±2.48	6.84±2.53	22.03±1.07	12.14±2.03
AnomalyBert [10]	23.99±1.22	2.77±0.12	13.38±0.67	13.36±2.21	11.79±1.56	6.26±5.50	7.14±3.09
CutAddPaste [13]	77.44±0.86	69.98±1.44	73.81±1.16	43.43±4.86	26.55±5.66	18.56±2.70	29.51±4.41
CAPMix	80.46±0.52	71.89±1.89	76.18±1.21	47.04±2.70	34.08±6.67	84.46±5.50	55.19±4.96

¹ Average RPA F1-score (%) with standard deviation for baselines and our method on AIOps, UCR, SWaT, WADI, and ESA datasets over 10 runs. The best results are in bold, and the suboptimal ones are underlined.

² SR could not be applied in multivariate time series anomaly detection.

and UCR datasets. For instance, the RPA F1 scores of COCA differ by 16% between the two univariate datasets. This divergence can be attributed to the predominant anomaly types in each dataset: point-wise anomalies for AIOps and pattern-wise ones for UCR. As a result, these methods exhibit varying sensitivity to specific types of anomalies. In contrast, our proposed method effectively strikes a relative balance between these two anomaly types, as indicated by its RPA F1 exceeding 70% on the two datasets. Secondly, multivariate TSAD is much more thorny, as indicated by the results on SWaT, WADI. Most methods fail to match the capabilities shown on univariate data sets. Even the method designed for multivariate data, such as Anomaly Transformer, can only achieve 32.91% on SWaT and performs much poorer on WADI as the dimension increases a lot. On the other hand, Anomaly Transformer does not perform well on univariate data sets, demonstrating that there are different emphases in univariate and multivariate TSAD tasks. Our approach obtains 47.04% and 34.08% F1 scores on SWaT and WADI, surpassing Anomaly Transformer by a large margin, indicating the progress CAPMix achieves. In addition, large-scale datasets such as ESA also highlight the model's ability to capture time series and computational time issues. The leading multi-dimensional anomaly detection methods did not achieve the expected excellent results, probably because the data in the 6-dimensional subset of ESA is strongly correlated, and the main difficulty is reflected in the ultra-long time series. Some other methods did not achieve results within an acceptable computational time. Our method achieved an F1-score of more than 80%, indicating that our steps did not significantly increase the computational overhead while

achieving great benefits.

Based on the comparison of the methods in the table, the following conclusions can be drawn. Firstly, among the traditional machine learning methods, DAMP and SR get RPA F1 of 39.03% and 22% on UCR, even surpassing some deep approaches. It indicates that the shallow methods could also work well in some specific cases, such as univariate pattern-wise anomalies. Nevertheless, they are defective in dealing with high-dimensional multivariate time series. Secondly, AOC and RoCA exhibit better performance than other baselines based on normality assumptions for TSAD. This implies that techniques involving reconstruction and incorporating multiple normality assumptions are more aligned with the nature of normal samples. In addition, TCC's unsatisfying results confirm the argument that pre-training limits the capability of the two-staged methods. Lastly, comparing the anomaly assumption-based methods, NCAD trails behind CutAddPaste in anomaly detection on all four datasets. On AIOps, NCAD manages to achieve a respectable F1 score exceeding 41% because it generates point-wise anomalies, consistent with the nature of the dataset. This reaffirms the potential of anomaly assumptions-based AD methods as a promising avenue. However, its gap with our CutAddPaste on the other datasets suggests that the injection of point anomalies and OE might struggle to handle complex pattern-wise anomalies effectively.

In summary, the proposed CAPMix method successfully balances point-wise and pattern-wise anomalies, generating highly discriminative anomaly scores and outperforming all baselines on all four datasets. This outcome underscores the

TABLE IV
ABLATION RESULTS¹.

Variants \ Dataset	Components			Univariate Datasets		Multivariate Datasets			Average
	AJ	LR	Mixup	AIOps	UCR	SWaT	WADI	ESA	
CAP	✓	×	×	77.44±0.86	69.98±1.44	43.43±4.86	26.55±5.67	18.56±2.70	47.19 (↓ 16.43)
CAP- γ	✓	✓	×	80.13±0.53	69.98±1.44	43.43±4.86	26.55±5.67	18.56±2.70	47.43 (↓ 16.10)
CAP- <i>mix</i>	✓	×	✓	78.15±0.86	68.65±2.45	47.04±2.70	34.08±6.67	84.46±6.67	62.48 (↓ 1.05)
CAPMix (full)	✓	✓	✓	80.19±0.50	71.89±1.89	47.04±2.70	34.08±6.67	84.46±6.67	63.53

¹ AJ refers to the process of anomaly injection via CutAddPaste. LR refers to label revision.

effectiveness and robustness of AD based on CutAddPaste augmentation.

D. Ablation Study

In this section, we study three variants, from a vanilla CutAddPaste to the full version of CAPMix. The ablation study about the three steps of CutAddPaste was carried out in the previous work. The RPA scores of these variants on the five datasets are shown in Table IV. The results reveal some insights into the effectiveness of our proposed method's components.

- **CAP.** The baseline method uses CutAddPaste anomaly injection with BCE loss. Note that results may be slightly different from the original version due to changes in loss and CUDA environments. On the large-scale ESA dataset, CAP performs poorly, possibly due to the large window size.
- **CAP- γ .** It applies hard-threshold label revision after anomaly injection via CutAddPaste. Samples within a γ -controlled distance to the normal center are assigned a uniform soft label of $1/\gamma$, indicating uncertainty.
- **CAP-Mix.** It applies dual-space Mixup to the injected samples, without any label revision. All samples are treated as fully anomalous with label 1.

We observe distinct behaviors in univariate and multivariate settings. The mechanism of label revision proves to be effective on univariate datasets (IOPsCompetition and UCR). Compared to baseline CAP, CAP- γ significantly improves the performance on AIOps, and the average of CAPMix rises 1.05% compared to CAP-*mix*, indicating that soft labels based on DTW distance help alleviate mislabeled synthetic anomalies that resemble normal data. These improvements confirm that in dealing with low-dimensional time series, where synthetic anomalies may appear similar to normal sequences, carefully calibrated labels are crucial. In contrast, CAP-*mix* shows little improvement, suggesting that Mixup between synthetic anomalies may disrupt temporal coherence in 1D signals, leading to unrealistic samples and reduced performance.

On multivariate datasets, the trend reverses. CAP-*mix* and the full version achieve significant improvements over CAP and CAP- γ , highlighting the effectiveness of dual-space Mixup in high-dimensional time series. In these cases, anomalies often emerge from correlations of the dimensions. Mixup

operations in both input and latent spaces enrich anomaly diversity and help the model generalize to complex, unexplored patterns. Meanwhile, label revision contributes little in this setting, likely because the DTW-based distance in multivariate time series fails to characterize holistic anomaly semantics accurately.

Overall, the full model CAPMix, combining both strategies, achieves the best or comparable performance across all datasets. This demonstrates the complementary nature of label revision and Mixup: the former improves supervision quality when synthetic anomalies resemble normal samples (univariate), while the latter enhances generalization by increasing structural diversity (multivariate). The flexibility to apply each component conditionally makes CAPMix adaptive across different anomaly detection settings. These results validate our design principle: anomaly synthesis must balance plausibility and diversity. Label revision ensures the former by avoiding overconfident supervision on borderline cases, while Mixup ensures the latter by augmenting rich intermediate representations. Their synergy enables robust learning under distribution shift and label uncertainty.

E. Robustness Analysis

To further evaluate the robustness of the proposed approach in realistic scenarios, we conduct a robust experiment on the AIOps dataset, which naturally contains anomalous samples in the training set. By repeatedly injecting additional real anomaly samples into the training set, we simulate different levels of training data corruption.

We plot the performance curves, including the F1-scores and precisions of CAPMix and the original CutAddPaste baseline as the corruption severity increases. As Fig.5 shows, the comparison reveals how well each method maintains detection performance when the training data is increasingly polluted with unseen or mislabeled anomalies. The results indicate that both CAPMix and the original CAP baseline exhibit strong resilience against increasing anomaly contamination in the training data. While CAP alone remains relatively stable across varying levels of corruption, CAPMix consistently outperforms it when the contamination becomes severe (e.g., at 8×). This suggests that the label revision and dual-space Mixup mechanisms further enhance the model's ability to handle heavily polluted or drifted data distributions, providing an extra layer of robustness where the vanilla CAP may start to degrade. In practice, this makes CAPMix a safer choice for

deployment in highly dynamic environments where the risk of data contamination or annotation noise is unavoidable.

F. Visualization

Detection results. To provide an intuitive qualitative evaluation, Fig. 6 shows the anomaly detection results of our approach on five datasets, covering both univariate (AIOps, UCR) and multivariate (SWaT, WADI, ESA) scenarios. The blue lines represent raw signals, and the red lines indicate the predicted anomaly scores, with green regions marking ground-truth anomalies. Qualitative analysis indicates that the model predicts a sequence of anomaly scores with better distinction, i.e., it's more sensitive to each type of anomaly.

For the AIOps dataset, the time series contains distinct point-wise anomalies that are relatively straightforward to detect. CAPMix generates clear peaks in the anomaly scores precisely aligned with these abnormal points, indicating its effectiveness in identifying sparse, point-wise deviations. Each sequence of UCR typically contains only one subtle pattern-wise anomaly that is more challenging to capture due to its low magnitude and short duration. The predicted anomaly scores show sharp peaks around the actual anomaly regions while maintaining lower scores for normal segments, demonstrating that CAPMix can sensitively detect pattern anomalies with minimal false positives. On industrial multivariate datasets, including SWaT and WADI, the model produces spikes that accurately reflect various short-duration anomalies within different sensor channels. This illustrates CAPMix's ability to capture system-level faults with complex interdependencies adaptively. Finally, for the ESA dataset, which is a large-scale multivariate dataset with sparse anomalies spread across long horizons, our method consistently highlights true anomalies with clear, distinguishable score spikes while remaining stable in normal regions. This demonstrates the scalability and reliability of CAPMix when applied to various scales of time-series data.

Alleviation of anomaly shift. To further analyze the anomalies produced by CAPMix and the original CutAddPaste, and

to get an intuitive feel for the role of the latter in anomaly drift correction, we plot the UMAP embeddings in Fig. 7. The purple \times s in the upper 5 figures are from CutAddPaste, and the orange stars are from CAPMix. The blue and red dots are the normal and anomalous in the test set.

Generally, CAPMix provides more pseudo-anomalies that are closer to the ground-truth anomalies in the test set, while almost not overlapping with the normal samples. The vanilla CutAddPaste generated more points that are disassociated with the dataset, especially in Fig 7(a), Fig 7(b), and Fig 7(e). It demonstrates that CAPMix manages to alleviate the issue of anomaly shift and helps the model classify well and identify anomalies mixed in normal data. A subtle phenomenon occurs that on the high dimensional SWaT and WADI, there are clusters of anomalies that are missed by both approaches, that are, the up left red dots in Fig 7(c) and Fig 7(h) and those at the left of Fig 7(d) and Fig 7(i). We would like to emphasize that this is due to the serious concept drift problem on these two datasets, rather than the anomaly drift problem of the generated anomalies. Therefore, this is not within the scope of this paper but will be addressed in our future work.

G. Hyperparameter Analysis

We conducted a sensitivity analysis to study the impact of hyperparameters, including the label revision range (γ) and the mixup ratio (α). Analysis of other crucial parameters, such as the degree of the trend term (ρ) and the minimum length of the patch (ζ), can be found in our previous work.

We chose two univariate and multivariate datasets to study the effects, since it may turn out to vary according to the dimension. Specifically, for each dataset, we fix γ at five different levels and sweep α across a meaningful range, then visualize the performance variations as shown in Fig. 8. Generally, the approach is sensitive to γ and α .

For the univariate AIOps dataset, the curves corresponding to different γ values are clearly separated, indicating that the choice of the revision boundary significantly affects performance. This confirms that the label revision mechanism effectively controls the impact of anomaly samples that are overly similar to normal data, which aligns well with our ablation results, where the label revision variant outperforms the original CAP baseline. Meanwhile, the relatively flat lines within each γ curve imply that the method is not highly sensitive to the Mixup ratio α in this setting. This suggests that, for univariate time-series anomalies, the benefit from input/latent space Mixup is limited, likely because the anomalies themselves are less complex and do not require additional synthetic diversity to cover the decision boundary effectively.

In contrast, for the multivariate WADI dataset, we observe that each γ curve exhibits more pronounced fluctuations with varying α . This indicates that the Mixup mechanism plays a much more important role in the multivariate case, helping to generalize the anomaly distribution under more complex inter-variable correlations. Furthermore, the separation between different γ curves remains visible, demonstrating that the label revision still contributes complementary improvements by constraining the plausibility of generated anomalies.

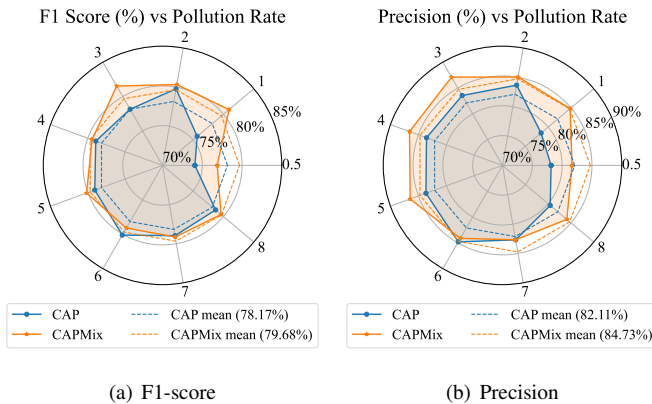


Fig. 5. Robustness evaluation of CAPMix and CutAddPaste (CAP) under varying levels of training set contamination. The plots show the changes in F1-score (left) and Precision (right) as the severity of corruption increases from 0.5x to 8x. The average scores across all contamination levels are also indicated, demonstrating the overall stability of CAPMix compared to CAP.

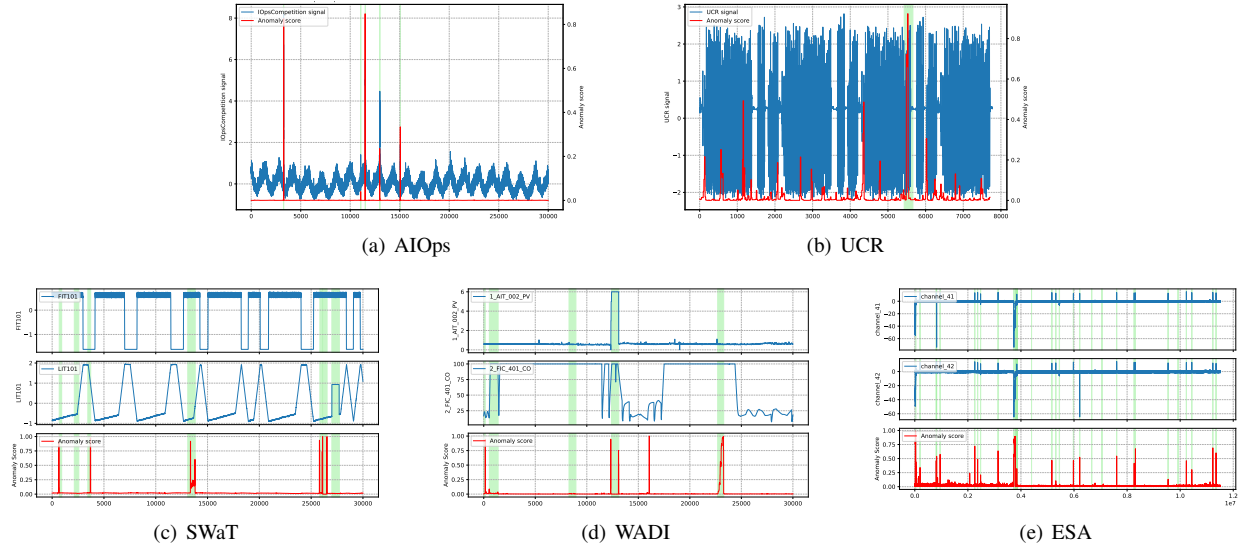


Fig. 6. The visualization of CAPMix AD results on the five datasets. The x-axis is timestamps, and the y-axis is signal values. The original data is present as the blue curves. For multivariate datasets, we plot 2 different dimensions. The green areas are ground-truth anomalies, including point- and pattern-wise ones. The red curves represent the anomaly scores predicted by our method.

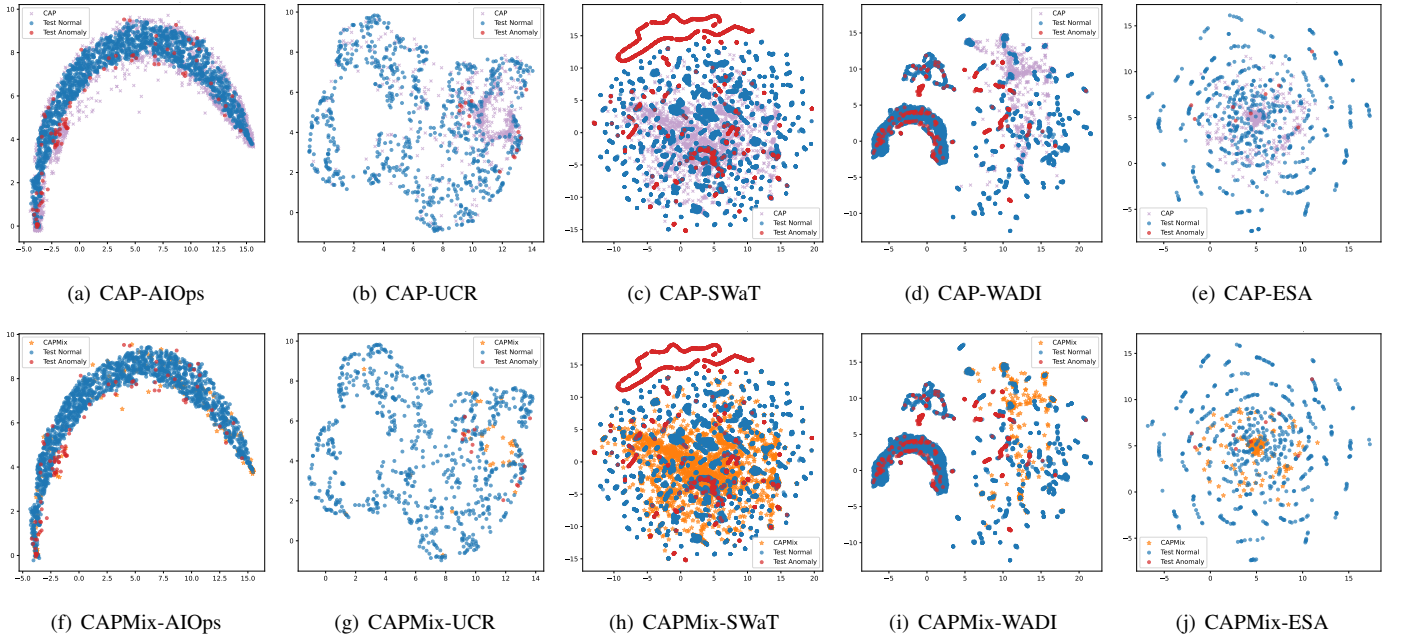


Fig. 7. UMAP comparison between synthetic samples generated by CAP (a-e) and CAPMix (f-j), with normal (blue) and real anomalous (red) test samples. The purple x are the anomalies injected by CutAddPaste, and the orange stars are from CAPMix. CAPMix shows significantly better alignment with real anomalies. It avoids overlap with normal regions and also prevents being excessively distant from the samples.

Overall, the analysis supports our design choices: the proposed label revision and dual-space Mixup are each beneficial but address different aspects of the anomaly shift problem. The impact of γ shows the importance of correcting label confidence for near-normal samples, while the sensitivity to α highlights the role of Mixup in increasing robustness for high-dimensional, complex scenarios.

V. DISCUSSION

Addressing anomaly shift remains a persistent challenge in anomaly detection methods that rely on synthetic sample

injection. CAPMix combines a label revision mechanism and Dual-Space Mixup to tackle this issue from two angles. However, several observations from our experiments reveal important open questions and directions for future work.

Dual-Space Mixup Design. While this work proposes a Dual-Space Mixup strategy that integrates mixup operations in both the input and latent representation spaces, our current ablation study does not fully disentangle their contributions due to limited space and computational cost. Future work will systematically examine the complementary roles and interactions between these two spaces by introducing additional controlled

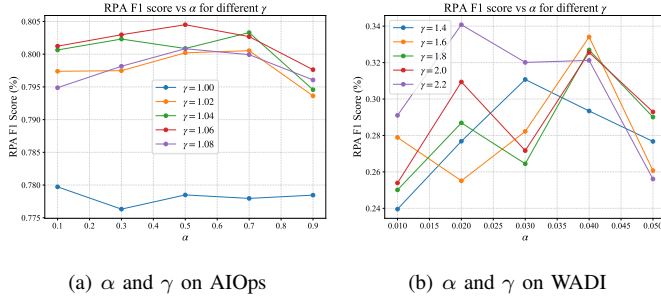


Fig. 8. Effect of different γ values (five lines) and α settings on the RPA F1 score. Each line represents one γ ; points along each line correspond to different α values.

baselines and more fine-grained visualizations. Such an analysis would provide deeper insight into how the input-space augmentation enhances sample diversity while the latent-space mixing regularizes internal representations, further clarifying their joint effect on mitigating anomaly shift.

Effectiveness of Label Revision. Our label revision mechanism, which softens the labels of normal-like synthetic anomalies, has shown clear benefits on univariate datasets. However, its impact on the heavily contaminated AIOPs dataset was relatively limited, suggesting that in scenarios with abundant real anomalies, the benefit of synthetic sample relabeling may diminish. A promising direction is to explore adaptive or data-driven revision thresholds that better align with real-world anomaly severity and distribution shifts.

Continuous vs Discrete Soft Labels. We find that coarse-grained soft labeling (e.g., $1/\gamma$) performs on par with more refined, distance-scaled labels in most cases, during experiments. This highlights a key trade-off between complexity and utility—more granular labels introduce theoretical appeal but may not yield significant performance gains in practice. Therefore, simple regularization may suffice, especially when the synthetic anomaly distribution is already well aligned.

VI. CONCLUSIONS

In this paper, we revisited the challenge of anomaly detection in time series data under limited and imbalanced labels, highlighting the often-overlooked Anomaly Shift issue that arises when synthetic anomalies deviate too much or too little from the normal distribution. To address this, we proposed CAPMix, a robust and unified framework that extends CutAddPaste with two key enhancements: a dynamic label revision mechanism based on DTW distance and a Dual-Space Mixup strategy integrated into a temporal convolutional network. This design encourages the generation of plausible yet diverse anomalies while preserving distributional integrity, leading to more reliable detection boundaries. Theoretical analysis provides insight into how our approach effectively mitigates distributional drift, and comprehensive experiments on both univariate and multivariate benchmarks demonstrate that CAPMix consistently outperforms strong baselines in terms of accuracy and robustness under varying contamination levels. We hope this work sheds new light on the limitations of anomaly injection methods and inspires further exploration of

flexible, distribution-aware augmentation strategies for robust time series anomaly detection.

REFERENCES

- [1] P. Malhotra, A. Ramakrishnan, G. Anand, L. Vig, P. Agarwal, and G. Shroff, "Lstm-based encoder-decoder for multi-sensor anomaly detection," *arXiv preprint arXiv:1607.00148*, 2016.
- [2] L. Ruff, R. Vandermeulen, N. Goernitz, L. Deecke, S. A. Siddiqui, A. Binder, E. Müller, and M. Kloft, "Deep one-class classification," in *International conference on machine learning*. PMLR, 2018, pp. 4393–4402.
- [3] R. Wang, C. Liu, X. Mou, K. Gao, X. Guo, P. Liu, T. Wo, and X. Liu, "Deep contrastive one-class time series anomaly detection," in *Proceedings of the 2023 SIAM International Conference on Data Mining (SDM)*. SIAM, 2023, pp. 694–702.
- [4] X. Mou, R. Wang, T. Wang, J. Sun, B. Li, T. Wo, and X. Liu, "Deep autoencoding one-class time series anomaly detection," in *ICASSP 2023-2023 IEEE International Conference on Acoustics, Speech and Signal Processing (ICASSP)*. IEEE, 2023, pp. 1–5.
- [5] X. Mou, R. Wang, B. Li, T. Wo, J. Sun, H. Wang, and X. Liu, "Roca: Robust contrastive one-class time series anomaly detection with contaminated data," *arXiv preprint arXiv:2503.18385*, 2025.
- [6] D. Hendrycks, M. Mazeika, and T. Dietterich, "Deep anomaly detection with outlier exposure," in *International Conference on Learning Representations*, 2018.
- [7] C.-L. Li, K. Sohn, J. Yoon, and T. Pfister, "Cutpaste: Self-supervised learning for anomaly detection and localization," in *Proceedings of the IEEE/CVF conference on computer vision and pattern recognition*, 2021, pp. 9664–9674.
- [8] L. Ruff, R. A. Vandermeulen, N. Goernitz, A. Binder, E. Müller, K.-R. Müller, and M. Kloft, "Deep semi-supervised anomaly detection," *arXiv preprint arXiv:1906.02694*, 2019.
- [9] C. U. Carmona, F.-X. Aubet, V. Flunkert, and J. Gasthaus, "Neural contextual anomaly detection for time series," *IJCAI*, 2022.
- [10] Y. Jeong, E. Yang, J. H. Ryu, I. Park, and M. Kang, "Anomalybert: Self-supervised transformer for time series anomaly detection using data degradation scheme," *arXiv preprint arXiv:2305.04468*, 2023.
- [11] K.-H. Lai, D. Zha, J. Xu, Y. Zhao, G. Wang, and X. Hu, "Revisiting time series outlier detection: Definitions and benchmarks," in *Thirty-fifth conference on neural information processing systems datasets and benchmarks track (round 1)*, 2021.
- [12] K. Hundman, V. Constantinou, C. Laporte, I. Colwell, and T. Soderstrom, "Detecting spacecraft anomalies using lstms and nonparametric dynamic thresholding," in *Proceedings of the 24th ACM SIGKDD international conference on knowledge discovery & data mining*, 2018, pp. 387–395.
- [13] R. Wang, X. Mou, R. Yang, K. Gao, P. Liu, C. Liu, T. Wo, and X. Liu, "Cutaddpaste: Time series anomaly detection by exploiting abnormal knowledge," in *Proceedings of the 30th ACM SIGKDD Conference on Knowledge Discovery and Data Mining*, 2024, pp. 3176–3187.
- [14] G. Pang, C. Shen, L. Cao, and A. V. D. Hengel, "Deep learning for anomaly detection: A review," *ACM Computing Surveys (CSUR)*, vol. 54, no. 2, pp. 1–38, 2021.
- [15] T. Schlegl, P. Seebock, S. M. Waldstein, U. Schmidt-Erfurth, and G. Langs, "Unsupervised anomaly detection with generative adversarial networks to guide marker discovery," in *International conference on information processing in medical imaging*. Springer, 2017, pp. 146–157.
- [16] X. Xia, X. Pan, N. Li, X. He, L. Ma, X. Zhang, and N. Ding, "Gan-based anomaly detection: A review," *Neurocomputing*, vol. 493, pp. 497–535, 2022.
- [17] B. Zong, Q. Song, M. R. Min, W. Cheng, C. Lumezanu, D. Cho, and H. Chen, "Deep autoencoding gaussian mixture model for unsupervised anomaly detection," in *ICLR*, 2018.
- [18] K. Sohn, C.-L. Li, J. Yoon, M. Jin, and T. Pfister, "Learning and evaluating representations for deep one-class classification," *ICLR*, 2021.
- [19] Z. Z. Darban, Q. Wang, G. I. Webb, S. Pan, C. C. Aggarwal, and M. Salehi, "Genias: Generator for instantiating anomalies in time series," *arXiv preprint arXiv:2502.08262*, 2025.
- [20] K. Obata, Y. Matsubara, and Y. Sakurai, "Robust and explainable detector of time series anomaly via augmenting multiclass pseudo-anomalies," 2025.
- [21] L. Ruff, R. A. Vandermeulen, B. J. Franks, K.-R. Müller, and M. Kloft, "Rethinking assumptions in deep anomaly detection," *arXiv preprint arXiv:2006.00339*, 2020.

- [22] H. Zhang, M. Cisse, Y. N. Dauphin, and D. Lopez-Paz, “mixup: Beyond empirical risk minimization,” *arXiv preprint arXiv:1710.09412*, 2017.
- [23] S. Yun, D. Han, S. J. Oh, S. Chun, J. Choe, and Y. Yoo, “Cutmix: Regularization strategy to train strong classifiers with localizable features,” in *Proceedings of the IEEE/CVF international conference on computer vision*, 2019, pp. 6023–6032.
- [24] S. Huang, X. Wang, and D. Tao, “Snapmix: Semantically proportional mixing for augmenting fine-grained data,” in *Proceedings of the AAAI conference on artificial intelligence*, vol. 35, no. 2, 2021, pp. 1628–1636.
- [25] J. Jeong, S. Park, M. Kim, H.-C. Lee, D.-G. Kim, and J. Shin, “Smoothmix: Training confidence-calibrated smoothed classifiers for certified robustness,” *Advances in Neural Information Processing Systems*, vol. 34, pp. 30 153–30 168, 2021.
- [26] V. Verma, A. Lamb, C. Beckham, A. Najafi, I. Mitliagkas, D. Lopez-Paz, and Y. Bengio, “Manifold mixup: Better representations by interpolating hidden states,” in *International conference on machine learning*. PMLR, 2019, pp. 6438–6447.
- [27] B. U. Demirel and C. Holz, “Finding order in chaos: A novel data augmentation method for time series in contrastive learning,” *Advances in Neural Information Processing Systems*, vol. 36, pp. 30 750–30 783, 2023.
- [28] S. Wang, J. Li, X. Shi, Z. Ye, B. Mo, W. Lin, S. Ju, Z. Chu, and M. Jin, “Timemixer++: A general time series pattern machine for universal predictive analysis,” *arXiv preprint arXiv:2410.16032*, 2024.
- [29] R. Wu and E. Keogh, “Current time series anomaly detection benchmarks are flawed and are creating the illusion of progress,” *IEEE Transactions on Knowledge and Data Engineering*, 2021.
- [30] A. Lavin and S. Ahmad, “Evaluating real-time anomaly detection algorithms—the numenta anomaly benchmark,” in *2015 IEEE 14th international conference on machine learning and applications (ICMLA)*. IEEE, 2015, pp. 38–44.
- [31] Yahoo, “S5 - a labeled anomaly detection dataset, version 1.0 (16m),” <https://webscope.sandbox.yahoo.com/catalog.php?datatype=s&did=70>, 2015, accessed: 2023-04-14.
- [32] Y. Su, Y. Zhao, C. Niu, R. Liu, W. Sun, and D. Pei, “Robust anomaly detection for multivariate time series through stochastic recurrent neural network,” in *Proceedings of the 25th ACM SIGKDD international conference on knowledge discovery & data mining*, 2019, pp. 2828–2837.
- [33] AIOps Challenge., “The 1st match for aiops,” <https://github.com/NetManAIOps/KPI-Anomaly-Detection>, 2018, accessed: 2023-04-14.
- [34] A. P. Mathur and N. O. Tippenhauer, “Swat: A water treatment testbed for research and training on ics security,” in *2016 international workshop on cyber-physical systems for smart water networks (CySWater)*. IEEE, 2016, pp. 31–36.
- [35] C. M. Ahmed, V. R. Palleti, and A. P. Mathur, “Wadi: a water distribution testbed for research in the design of secure cyber physical systems,” in *Proceedings of the 3rd international workshop on cyber-physical systems for smart water networks*, 2017, pp. 25–28.
- [36] K. Kotowski, C. Haskamp, J. Andrzejewski, B. Ruszczak, J. Nalepa, D. Lakey, P. Collins, A. Kolmas, M. Bartesaghi, J. Martinez-Heras *et al.*, “European space agency benchmark for anomaly detection in satellite telemetry,” *arXiv preprint arXiv:2406.17826*, 2024.
- [37] H. Xu, W. Chen, N. Zhao, Z. Li, J. Bu, Z. Li, Y. Liu, Y. Zhao, D. Pei, Y. Feng *et al.*, “Unsupervised anomaly detection via variational auto-encoder for seasonal kpis in web applications,” in *Proceedings of the 2018 World Wide Web Conference*, 2018, pp. 187–196.
- [38] S. Kim, K. Choi, H.-S. Choi, B. Lee, and S. Yoon, “Towards a rigorous evaluation of time-series anomaly detection,” in *Proceedings of the AAAI Conference on Artificial Intelligence*, vol. 36, 2022, pp. 7194–7201.
- [39] A. Huet, J. M. Navarro, and D. Rossi, “Local evaluation of time series anomaly detection algorithms,” in *ACM SIGKDD*, 2022, pp. 635–645.
- [40] B. Schölkopf, R. C. Williamson, A. J. Smola, J. Shawe-Taylor, J. C. Platt *et al.*, “Support vector method for novelty detection,” in *NIPS*, vol. 12. Citeseer, 1999, pp. 582–588.
- [41] F. T. Liu, K. M. Ting, and Z.-H. Zhou, “Isolation-based anomaly detection,” *ACM Transactions on Knowledge Discovery from Data (TKDD)*, vol. 6, no. 1, pp. 1–39, 2012.
- [42] S. Guha, N. Mishra, G. Roy, and O. Schrijvers, “Robust random cut forest based anomaly detection on streams,” in *ICML*. PMLR, 2016, pp. 2712–2721.
- [43] H. Ren, B. Xu, Y. Wang, C. Yi, C. Huang, X. Kou, T. Xing, M. Yang, J. Tong, and Q. Zhang, “Time-series anomaly detection service at microsoft,” in *ACM SIGKDD*, 2019, pp. 3009–3017.
- [44] Y. Lu, R. Wu, A. Mueen, M. A. Zuluaga, and E. Keogh, “Matrix profile xxiv: scaling time series anomaly detection to trillions of datapoints and ultra-fast arriving data streams,” in *Proceedings of the 28th ACM SIGKDD Conference on Knowledge Discovery and Data Mining*, 2022, pp. 1173–1182.
- [45] E. Eldele, M. Ragab, Z. Chen, M. Wu, C. K. Kwok, X. Li, and C. Guan, “Time-series representation learning via temporal and contextual contrasting,” *IJCAI*, 2021.
- [46] J. Xu, H. Wu, J. Wang, and M. Long, “Anomaly transformer: Time series anomaly detection with association discrepancy,” in *International Conference on Learning Representations*, 2021.
- [47] K. Alkilane, Y. He, and D.-H. Lee, “Mixmamba: Time series modeling with adaptive expertise,” *Information Fusion*, vol. 112, p. 102589, 2024.
- [48] H. Si, C. Pei, Z. Li, Y. Zhao, J. Li, H. Zhang, Z. Diao, J. Li, G. Xie, and D. Pei, “Beyond sharing: Conflict-aware multivariate time series anomaly detection,” in *Proceedings of the 31st ACM Joint European Software Engineering Conference and Symposium on the Foundations of Software Engineering*, 2023, pp. 1635–1645.
- [49] Y. Feng, W. Zhang, Y. Fu, W. Jiang, J. Zhu, and W. Ren, “Sensitivehue: Multivariate time series anomaly detection by enhancing the sensitivity to normal patterns,” in *Proceedings of the 30th ACM SIGKDD Conference on Knowledge Discovery and Data Mining*, 2024, pp. 782–793.
- [50] A. Bhatnagar, P. Kassianik, C. Liu, T. Lan, W. Yang, R. Cassius, D. Sahoo, D. Arpit, S. Subramanian, G. Woo *et al.*, “Merlion: A machine learning library for time series,” *arXiv preprint arXiv:2109.09265*, 2021.